Structural and optical properties of AgCl-sensitized TiO_2 (TiO_2@AgCl) prepared by a reflux technique under alkaline condition

(Propriedades estruturais e ópticas de TiO_2 sensibilizado com AgCl (TiO_2@AgCl) preparado por técnica de refluxo em condição alcalina)

V. A. Mu'izayanti[1], H. Sutrisno[1]*

[1]Universitas Negeri Yogyakarta, Faculty of Mathematics and Natural Sciences, Department of Chemistry Education, Campus Karangmalang, Jl. Colombo No. 1, Yogyakarta, 55281, Indonesia

Abstract

The AgCl-sensitized TiO_2 (TiO_2@AgCl) has been prepared from the precursor of TiO_2-rutile type which on its surface adsorb chloride anion (Cl^-) and various amounts of silver using $AgNO_3$ as starting material: $AgNO_3/(AgNO_3+TiO_2)$ mass ratio of 0.00, 1.14, 3.25, 6.38 and 10.32%. Reflux under alkaline condition was the employed technique. All samples were characterized by X-ray diffraction (XRD) and diffuse reflectance UV-vis spectroscopy. The sample without the addition of $AgNO_3$ was analyzed by scanning electron microscope and surface area analyzer. The morphology of the sample showed a distribution of microspheres of approximately 0.5 to 1.0 μm and the specific surface area was 68 m^2/g. XRD patterns indicated that the sample without the addition of $AgNO_3$ contained two types of TiO_2: rutile (major) and anatase (minor), whereas the samples with the addition of $AgNO_3$ consisted of one phase of AgCl and two types of TiO_2: rutile and anatase. The bandgaps of the samples were in the range of 2.97 to 3.24 eV, which were very close to the bandgap of intrinsic TiO_2 powder. The presence of 0.8, 2.6 and 4.4 wt% of AgCl in each sample resulted in an additional bandgap in visible light region of 1.90, 1.94 and 2.26 eV, respectively, whereas the presence of 9.4 wt% of AgCl in the sample resulted in two bandgaps in visible light region of 1.98 and 1.88 eV.

Keywords: TiO_2, anatase, rutile, AgCl, bandgap, alkaline condition.

Resumo

O TiO_2 sensibilizado com AgCl (TiO_2@AgCl) foi preparado a partir do precursor de tipo TiO_2-rutilo que na sua superfície adsorve o ânion cloreto (Cl^-) e várias quantidades de prata utilizando $AgNO_3$ como material de partida: relação de massa $AgNO_3/(AgNO_3+TiO_2)$ de 0,00, 1,14, 3,25, 6,38 e 10,32%. O refluxo em condições alcalinas foi a técnica empregada. Todas as amostras foram caracterizadas por difração de raios X (DRX) e espectroscopia UV-vis de reflectância difusa. A amostra sem adição de $AgNO_3$ foi analisada em microscópio eletrônico de varredura e analisador de área de superfície. A morfologia da amostra mostrou uma distribuição de microesferas de aproximadamente 0,5 a 1,0 μm e a área superficial específica foi de 68 m^2/g. Os difratogramas de DRX indicaram que a amostra sem adição de $AgNO_3$ continha dois tipos de TiO_2: rutilo (principal) e anatásio, enquanto as amostras com adição de $AgNO_3$ apresentaram uma fase de AgCl e dois tipos de TiO_2: rutilo e anatásio. As energias da banda proibida (bandgaps) das amostras foram na faixa de 2,97 a 3,24 eV, muito próximas da bandgap de TiO_2 intrínseco. A presença de 0,8, 2,6 e 4,4% em massa de AgCl em cada amostra resultou em bandgap adicional na região da luz visível de 1,90, 1,94 e 2,26 eV, respectivamente, enquanto a presença de 9,4% em massa de AgCl na amostra resultou em dois bandgaps na região da luz visível de 1,98 e 1,88 eV.

***Palavras-chave**: TiO_2, anatásio, rutilo, AgCl, bandgap, condição alcalina.*

INTRODUCTION

Among semiconductor materials, titania or titanium dioxide (TiO_2) is expected to play an important role in 21st century's efforts in applications as a photocatalyst [1], solar cells [2], anti-fogging [3], antibacterial [4], anti-fungals [5], a white powder pigment [6], and wastewater cleaning [7]. TiO_2 can be applied in everyday life because of its brightness, very high refractive index, absence of toxicity, high chemical stability, inert and high photocatalytic. The photoactivity of TiO_2 is characterized by a photoinduced phenomena which is consequence of TiO_2 bandgap. The TiO_2 can absorb photons when photons have a higher energy ($h\nu$) than this band gap, and an electron (e^-) is promoted to the conduction band (CB), then leaving a hole (h^+) in the valence band (VB). This excited electron can either be used directly to create electricity in photovoltaic solar cells or drive a chemical reaction, which is called photocatalysis. A special phenomenon was recently discovered: trapping of holes at the TiO_2 surface causes a high wettability and is termed photoinduced super hydrophilicity (PSH). PSH involves reduction of Ti(IV) cations to Ti(III) by electrons and simultaneous trapping of holes at lattice sites or close to the surface of the semiconductor (TiO_2) [8].

The bandgap in a semiconductor is influenced by variables, such as particle size, morphology, crystallinity

**sutrisnohari@uny.ac.id*

and crystal structure. In fact, TiO_2 has 11 types of structure (polymorphs). Three of them occur in nature in the form of minerals: anatase, rutile, and brookite [9]. Kinetically, anatase is stable, but it transforms into rutile for bulk TiO_2 at temperature >600 °C [10]. The anatase has a bandgap of 3.2 eV, while bandgap is 3.0 eV for rutile and 3.4 eV for brookite [11]. All types of TiO_2 can only absorb photons in the ultraviolet region: 200 to 400 nm, so as TiO_2 do not have a response in the visible region [12]. Sunlight has a 5% emission of ultraviolet rays reaching the earth's surface [13]. Therefore, some efforts are necessary to increase the TiO_2 photoactivity, among others, by controlling the particle size, morphology and structure type, so as to reduce the bandgap to be active in the visible region.

TiO_2 can be synthesized by various methods. Some researches have been done to improve the efficiency of the photoactivity of TiO_2 photocatalyst, including the synthesis of nanocrystalline TiO_2 [14], the insertion of dopant [15], and the addition of sensitizer [16]. Dopant and sensitizer, which are commonly used, include vanadium [17], nitrogen [18], cadmium sulfide [16], gold [19], and zinc sulfide [20]. Silver chloride (AgCl) is one of the most widely used sensitizer on TiO_2. Yang *et al*. [21] successfully added Ag/AgCl and porous magnesia (PM) or imporous magnesia (IM) on the surface of TiO_2 *in-situ*. The results showed that the photocatalytic activity of the benzene gas decomposition of Ag/AgCl/TiO_2/PM was 5.21 times higher than TiO_2/PM and 30.57 times higher than TiO_2/IM. These results suggest that silver chloride may act as sensitizer substance that can be used as a photocatalyst. Sangcay *et al*. [22] synthesized TiO_2@AgCl by sol-gel method and calcined between 400-600 °C; the sample calcined at 400 °C for 2 h had the highest concentration of anatase and smallest diameter. The main goal of this work was the investigation of the influence of amount of AgCl (sensitizer) on the surface of titanium dioxide to the structural and optical properties. The AgCl-sensitized titanium dioxide (TiO_2@AgCl) was obtained using a reflux technique under alkaline conditions.

MATERIALS AND METHODS

Materials. For the synthesis, silver nitrate ($AgNO_3$, 99.9%), hydrogen peroxide (H_2O_2), and ammonium hydroxide (NH_4OH) were procured from Merck. Titanium tetrachloride ($TiCl_4$, 97%), tetramethylammonium hydroxide [$(CH_3)_4NOH$] and paraffin oil were obtained from Sigma-Aldrich. Commercial TiO_2-anatase and TiO_2-rutile were supplied from Sigma-Aldrich in order to compare their characteristics with the powders synthesized in the present study. All the reagents were analytical grade and used for the synthesis without any further purification.

Preparation of precursor and AgCl-sensitized TiO_2 (TiO_2@AgCl): the precursor (TiO_2) was obtained by hydrolysis of titanium tetrachloride. A total of 100 mL of $TiCl_4$ solution was poured into a 1 L beaker glass. Then a solution of H_2O_2 was added dropwise to a solution of $TiCl_4$ to form a yellowish white precipitate. Hydrogen peroxide plays a key role in the oxidation reaction. The reaction was strongly exothermic and produced high quantities of HCl fumes. The precipitate was filtered and dried in an oven at a temperature of 80 °C for 3 h, then characterized by X-ray diffraction (XRD). The precursor in this research was TiO_2 of rutile type which on its surface adsorb chloride anion (Cl^-). A number of the synthesized precursor (TiO_2-rutile) was dispersed into 50 mL of distilled water in beaker glass. Furthermore the emulsion was stirred for 1 h with a magnetic stirrer. In a separate beaker glass, a number of $AgNO_3$ was dissolved in 50 mL of distilled water. Furthermore, the emulsion of the precursor and the $AgNO_3$ solution were mixed in the boiling flask. The initial compositions of the precursor (TiO_2-rutile) and $AgNO_3$ used in this research are shown in Table I. In each mixture was added 1 mL of tetramethylammonium hydroxide and dropwise 8 M NH_4OH to pH ~10. The mixture was stirred with a magnetic stirrer and heated to 150 °C in the reflux equipment for 6 h. The resulting mixture was cooled under reflux for ~24 h. The resulting mixture was filtered with an alumina filter, then dried by oven at 110 °C overnight. These solids were characterized by XRD and diffuse reflectance ultra-violet (DR-UV) spectrophotometer.

Table I - Initial compositions of precursor (TiO_2-rutile) and $AgNO_3$.
[Tabela I - Composições iniciais de precursor (TiO_2-rutilo) e $AgNO_3$.]

Sample code	$AgNO_3$ (g)	Precursor (TiO_2-rutile) (g)	$\frac{AgNO_3}{(AgNO_3+TiO_2)}$(%)
TiAg-0	0.000	5.000	0.00
TiAg-1	0.057	4.899	1.14
TiAg-2	0.162	4.809	3.25
TiAg-3	0.319	4.672	6.38
TiAg-4	0.516	4.500	10.32

Characterization: after synthesis process, the prepared samples were examined for the investigation of phases or structure. The XRD patterns of samples were recorded with the powder X-ray diffractometer (Rigaku, Miniflex 600) with CuKα radiation (λ= 1.5406 Å) with operating voltage of 40 kV, current of 15 mA, 2θ angle range between 20 to 80°, and speed of 2° per min observation. Based on the results of XRD patterns the type of structure of TiO_2@AgCl was shown. The XRD results were further analyzed by U-Fit program to determine the lattice parameters (a, b, c) and cell volume for each sample [23]. The particle morphology and size of the sample without the addition of $AgNO_3$ were estimated from scanning electron microscopy (SEM, Coxem, EM-30AX) images. The Brunauer-Emmett-Teller (BET) specific surface area (S_{BET}) was carried out at 77 K with a Micromeritics ASAP 2020 instrument. The S_{BET} data were collected based on adsorption data (5 point) in the multi-point BET measurement from (P/P_0) of ~0.06 to ~0.30 [24].

In this research, quantitative analysis of XRD data refers

to the determination of amounts of different phases in multi-phase samples by using reference intensity ratio (RIR) method. The RIR is a method used for quantitative analysis by powder XRD and is based upon scaling all diffraction data to the diffraction of standard reference materials. Klug and Alexander were first to describe a technique for quantification using intensities of the crystalline phases in a mixture [25, 26]. General formula for relating intensity ratio to mass fraction is:

$$\frac{I_{(hkl)A}}{I_{(hkl)'B}} = k\frac{X_A}{X_B} \quad (A)$$

where: I - intensity, k - any other component in the unknown sample, X_A - weight fraction of phase A, X_B - weight fraction of phase B (corundum).

For the optical measurements, DR-UV spectra were obtained for the dry-pressed disk samples using a Shimadzu spectrophotometer UV-1770 specular reflectance with diffuse reflectance UV ISR-240A. This method is based on measurements of UV-vis intensity reflected by the sample. The measured reflectance is the reflectance expressed by:

$$R(h\nu) = \frac{R(h\nu)\ (sample)}{R(h\nu)\ (standard)} \quad (B)$$

This value was used to determine the Kubelka-Munk equation by [27-30]:

$$F(R(h\nu)) = \frac{[1 - R(h\nu)^2]}{[1 - R(h\nu)]} \quad (C)$$

Eq. C has a relationship with the parameter α - absorbance coefficient and s - diffusion reflectance scattering coefficient, while $F(R(h\nu))=\alpha/s$, so Eq. D can be written [31]:

$$F(R(h\nu))\ \frac{\alpha}{s} = \frac{[1 - R(h\nu)^2]}{2R(h\nu)} \quad (D)$$

The UV-vis spectra of diffuse reflectance yield a relation curve between α/s with wavelength (λ) or absorbance (A) with wavelength (λ). α corresponds to the photon energy expressed by [32]:

$$\alpha = A(E - Eg)^{\gamma} \quad (E)$$

with A being a constant dependent on the properties of the material, E is the energy of the photon, Eg is the bandgap and γ is a constant that has different values depending on the type of electronic transition. Next the equation becomes:

$$F(R(h\nu)) = \frac{\alpha}{s} = \frac{A(E-Eg)^{\gamma}}{s} \quad (F)$$

For a direct transition (a permitted direct transition), the value of γ=½, so the equation becomes:

$$F(R(h\nu))^2 = \left(\frac{A}{s}\right)^2 (E-Eg) \quad (G)$$

while the indirect transition (a permitted indirect transition), the value of γ=2, so the equation becomes:

$$F(R(h\nu))^{0.5} = \left(\frac{A}{s}\right)^{0.5} (E-Eg) \quad (H)$$

The value of hν is determined by equation:

$$Eg = h\nu = \frac{hc}{\nu} \quad (I)$$

with, Eg - band gap energy, h - Planck constant, c - speed of light, ν - frequency, and λ is the wavelength, so the equation becomes:

$$F(R(h\nu))^{0.5} = \left(\frac{A}{s}\right)^{0.5} (h\nu-Eg) \quad (J)$$

The calculation is performed on each sample using the Kubelka-Munk equation where Eg is obtained from the graph of the relationship between hν and $F(R(h\nu))^{1/2}$. The bandgap energy (Eg) is the value of hν at $F(R(h\nu))^{1/2}=0$ obtained from the linear equation of the curve.

RESULTS AND DISCUSSION

X-ray diffraction analysis: XRD pattern of the precursor is depicted in Fig. 1. The positions of all diffraction lines corresponded to rutile crystalline phase which is in agreement with the result of U-Fit analysis. The U-Fit analysis showed that the precursor had a tetragonal crystal system and a spatial group P, with lattice parameters: a= 4,6308 Å and c= 2.9898 Å. This result was identical to the TiO_2 crystal of the rutile type described in [33], which has a tetragonal crystal system with space group $P4_2/mnm$ and lattice parameters: a= 4.6344 Å and c= 2.9919 Å. The diffraction peaks at about 27.20, 35.68, 40.83, 43.64, 53.79, 56.10, 61.99 and 69.00° were perfectly indexed to the (110), (101), (111), (210), (211), (220), (002) and (112) reflections of rutile. The formation of rutile from the reaction of $TiCl_4$ with H_2O_2 is due to the reaction conditions in acidic conditions (very low pH) or high concentration of H^+ cations [34]. The results of the U-Fit analysis of the precursor (rutile) is summarized in Table II.

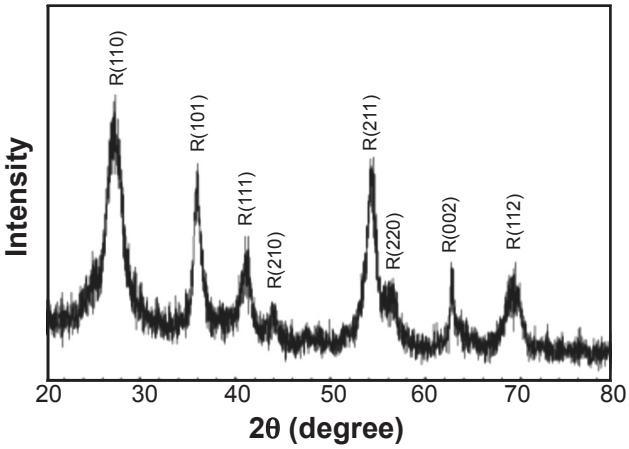

Figure 1: Powder X-ray diffraction pattern of precursor (TiO_2-rutile).
[Figura 1: Difratograma de raios X do precursor (TiO_2-rutilo).]

Table II - X-ray powder diffraction data of rutile (precursor).
[Tabela II - Dados de DRX (precursor).]

(hkl)	2θobs	2θcor	2θcalc	Δ(2θ)	Int. (I/I_o)
110	27.20	27.223	27.212	-0.011	100
101	35.68	35.703	35.718	0.015	58
111	40.83	40.853	40.838	-0.015	25
210	43.64	53.663	43.673	0.010	7
211	53.79	53.813	53.805	-0.008	71
220	56.10	56.123	56.132	0.010	20
002	61.99	62.013	62.032	0.019	28
112	69.00	69.023	69.005	-0.018	23
Lattice parameters			a= 4.6308 Å; c= 2.9898 Å		
Bravais lattice			P		
Volume			64.1137 $Å^3$		
Figure of merit*			D= 0.0132; R= 0.0174		

** - Characteristic factor of the refinement (D) is the mean deviation between $2\theta_{obs}$ and $2\theta_{calc}$, that is* $D=\frac{1}{n_{hkl}}\sum|(2)$ *, and the confidence factor (R) is given by* $R=\frac{1}{n_{hkl}-n_{var}}\sum(2\theta_{obs}-2\theta_{calc})^2$*, where n_{hkl} is the number of reflections taken into account and n_{var} is the number of refined variables.*

Fig. 2 shows the XRD patterns of all samples of AgCl-sensitized TiO_2. The XRD pattern (Fig. 2a) indicated that the TiAg-0 sample (without the addition of $AgNO_3$) contained two types of TiO_2: rutile (major) and anatase (minor). All samples with the addition of $AgNO_3$ (TiAg-1 to TiAg-4) consisted of one phase of AgCl and two types of TiO_2: rutile and anatase. The diffraction peaks at about 27.85, 32.16, 46.17, 54.80, 57.40, 67.43, 74.40 and 76.73° were perfectly indexed to the (111), (200), (220), (311), (222), (400), (331) and (420) reflections of a cubic structure of AgCl, which was identified using the standard data (PDF file No. 01-085-1355). The main diffraction peaks at about 25.30, 37.80, 38.60, 48.00, 53.93, 62.74 and 70.23° were indexed as the (101), (004), (112), (200), (105), (204) and

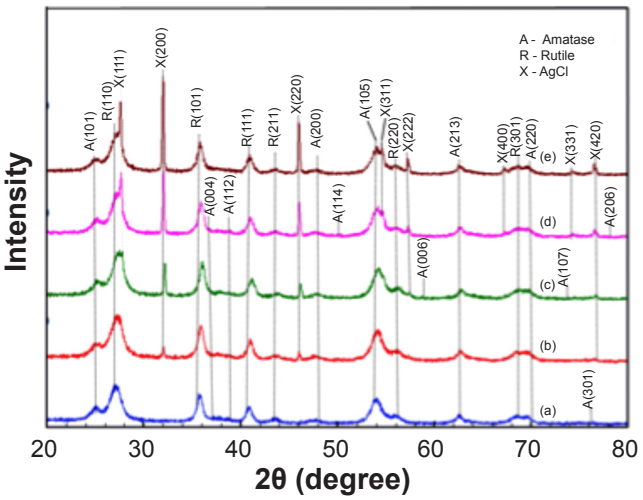

Figure 2: Powder X-ray diffraction patterns of TiO_2@AgCl samples: (a) TiAg-0, (b) TiAg-1, (c) TiAg-2, (d) TiAg-3, and (e) TiAg-4.
[Figura 2: Difratogramas de raios X das amostras de TiO_2@AgCl: (a) TiAg-0, (b) TiAg-1, (c) TiAg-2, (d) TiAg-3 e (e) TiAg-4.]

(220) reflections of crystalline anatase phase (tetragonal crystal system), corresponding to those shown in the PDF file No. 01-083-2243. The exhibited peaks at about 27.16, 35.67, 40.86, 43.65, 56.07 and 68.26° corresponded to the (110), (101), (111), (210), (220) and (301) of a tetragonal rutile structure of TiO_2, which was identified using the standard data (PDF file No. 01-076-0322). The U-Fit analysis showed that the AgCl phase has a cubic crystal system with Bravais lattice F, while the anatase phase has a tetragonal crystalline system with Bravais lattice I, and then the rutile phase has a tetragonal crystal system with Bravais lattice P. The lattice parameters and figure of merit were obtained by U-Fit analysis (Table III). The TiAg-0 consisted of two types of TiO_2 phases: anatase (minor) and rutile (major), while the samples of TiAg-1 to TiAg-4 consisted of three phases: anatase, rutile and AgCl. The anatase had a lattice parameter identical to the lattice parameter of anatase presented in [35], with unit cell: a= 3.7800 Å, c= 9.5100 Å,

Table III - Phase, Bravais lattice and unit cell parameters of TiO_2@AgCl samples.
[Tabela III - Fase, rede de Bravais e parâmetros de célula unitária das amostras de TiO_2@AgCl.]

Phase	Anatase			Rutile			AgCl	
Bravais lattice	I			P			F	
Sample code	a (Å)	c (Å)	V ($Å^3$)	a (Å)	c (Å)	V ($Å^3$)	a (Å)	V ($Å^3$)
TiAg-0	3.7824	9.5120	136.090	4.6303	2.9899	64.105	-	-
TiAg-1	3.7864	9.5036	136.253	4.6358	2.9893	64.246	5.5503	170.984
TiAg-2	3.7838	9.5118	136.187	4.6349	2.9897	64.227	5.5465	170.639
TiAg-3	3.7822	9.5052	135.976	4.6345	2.9896	64.217	5.5501	170.960
TiAg-4	3.7839	9.5172	136.273	4.6384	2.9917	64.369	5.5503	170.988
Figure of merit*	D= 0.0132; R= 0.0174			D= 0.0132; R= 0.0174			D= 0.0132; R= 0.0174	

** - See footnote in Table II.*

Table IV - Phase compositions of the samples (in wt%).
[Tabela IV - Composições de fases das amostras (em % em massa).]

Sample code	AgCl	Anatase	Rutile
TiAg-0	0.0	15.0	85.0
TiAg-1	0.8	18.0	81.2
TiAg-2	2.6	17.4	80.0
TiAg-3	4.4	16.6	79.0
TiAg-4	9.4	22.1	68.5

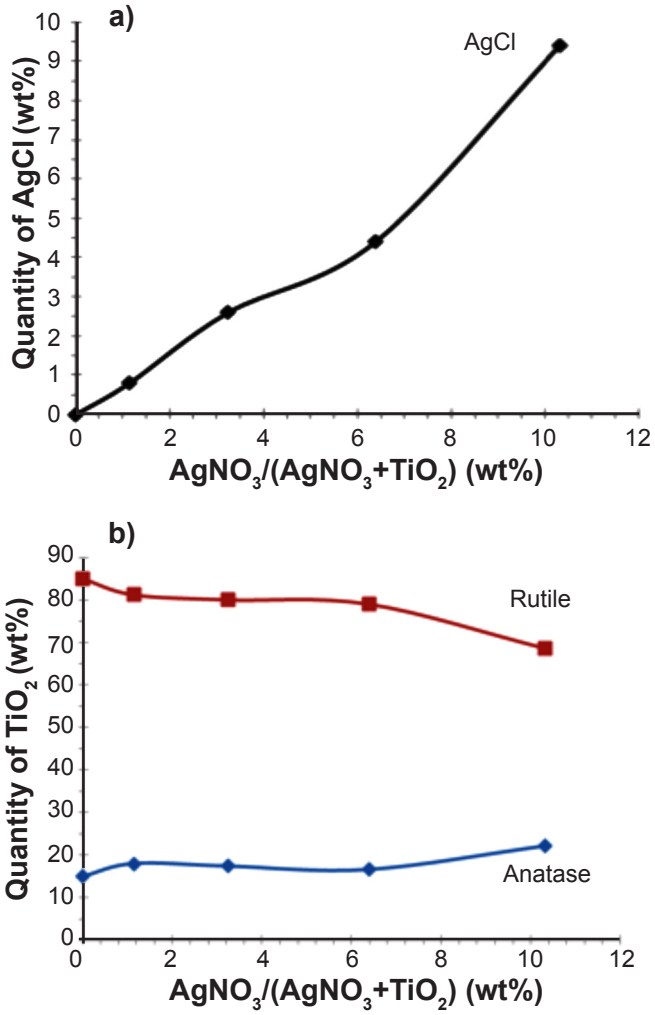

Figure 3: AgCl, anatase and rutile phase contents as a function of added $AgNO_3$ fraction.
[Figura 3: Teores das fases AgCl, anatásio e rutilo em função da fração de $AgNO_3$ adicionada.]

which has a tetragonal crystal system and the space group $I4_1/amd$. The rutile lattice parameters corresponded to the lattice parameters found in [33], with unit cell: a= 4.6344 Å, c= 2.9919 Å, which has a tetragonal crystal system and the space group $P4_2/mnm$, and the AgCl lattice parameters were identical to those lattice parameters in [36,] with a= 5.549 Å, which has a cubic crystal system and space group *Fm-3m*. The result of quantitative analysis with RIR method for

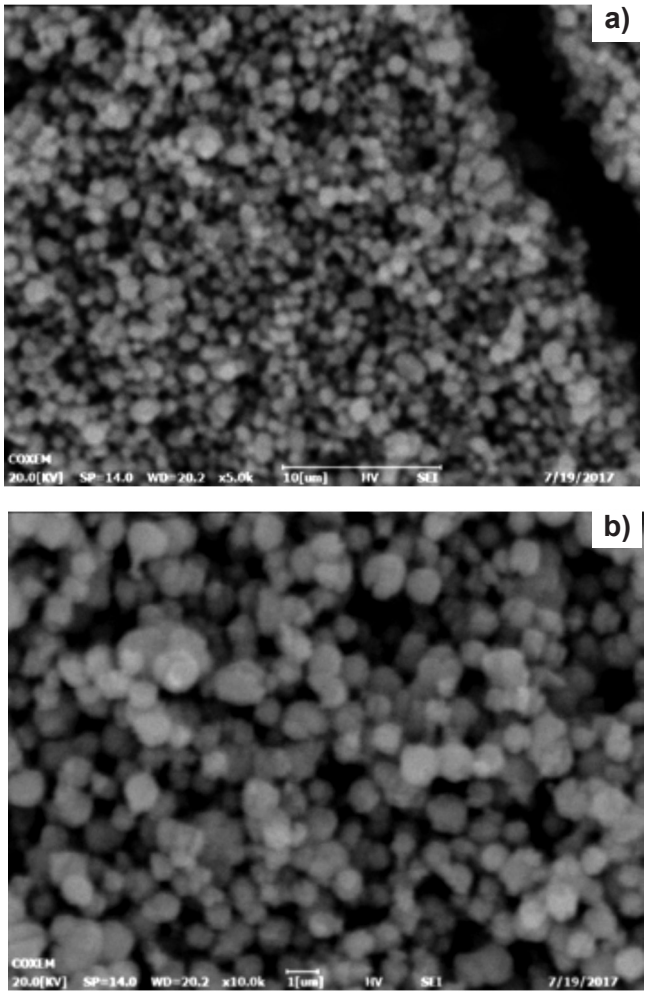

Figure 4: SEM images of prepared TiO_2 (TiAg-0).
[Figura 4: Micrografias obtidas por microscopia eletrônica de varredura do TiO_2 preparado (TiAg-0).]

Table V - Specific surface area (S_{BET}) of various TiO_2.
[Tabela V - Área de superfície específica (S_{BET}) de diversos TiO_2.]

Catalyst	Surface area (m^2/g)
TiO_2 anatase (Sigma-Aldrich)	52
TiO_2 rutile (Sigma-Aldrich)	48
Prepared TiO_2 (TiAg-0)	68

AgCl, anatase and rutile of each sample is shown in Table IV. The addition of $AgNO_3$ to the precursor (rutile) resulted in an increase in the quantity of AgCl, and the fraction of anatase phase tended to increase, whereas the fraction of rutile phase tended to decrease (Fig. 3).

Morphologies and specific surface area: shape and morphology were clearly observed in the SEM images of TiO_2 particles. Fig. 4 shows SEM images of TiAg-0 in two magnifications. As can be seen, there is a distribution of microsphere ranging approximately from 0.5 to 1.0 μm. Specific surface area (S_{BET}) of TiO_2-anatase, TiO_2-rutile and prepared TiO_2 (TiAg-0) were analyzed by using Brunauer-

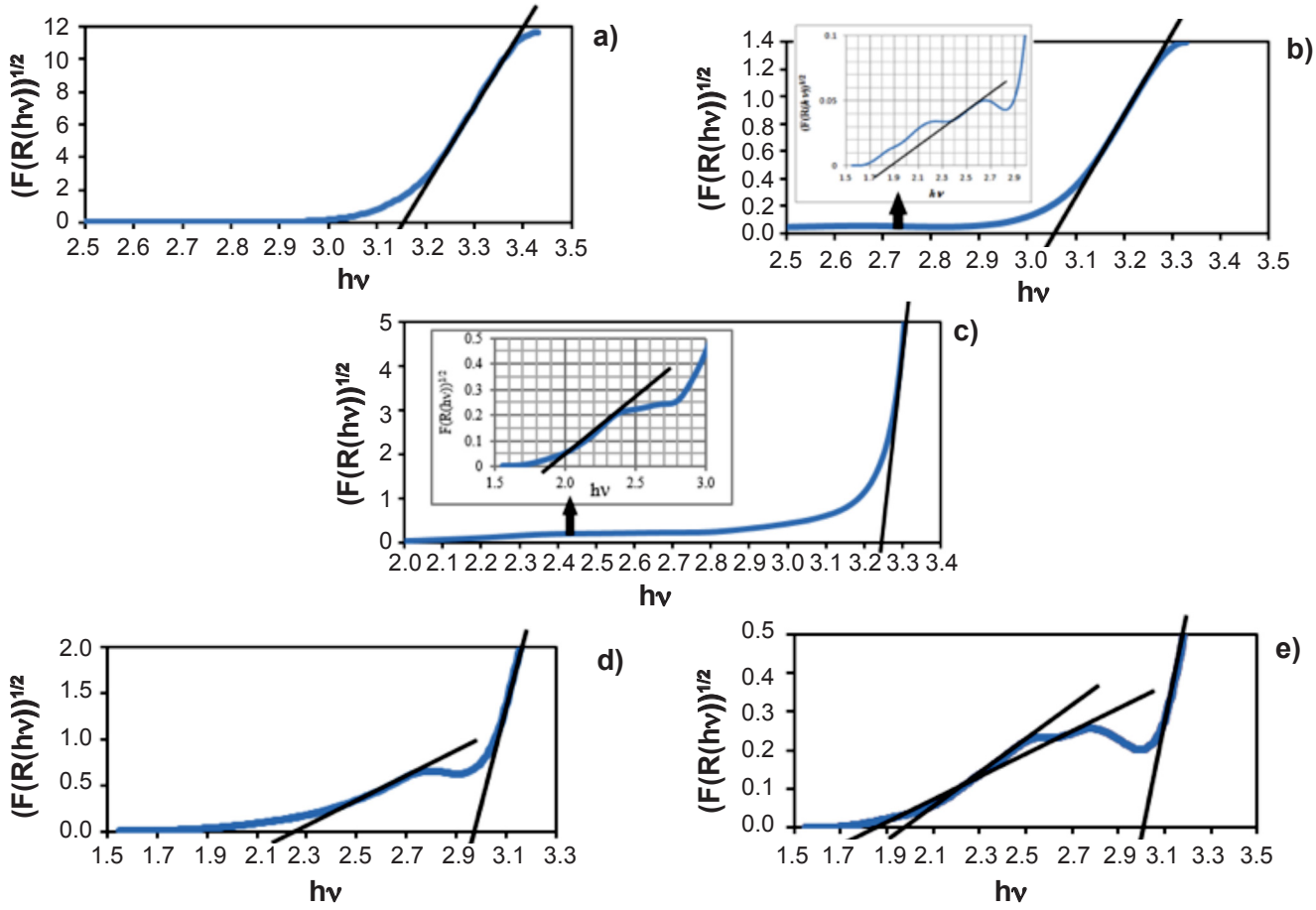

Figure 5: $F(R(h\nu))^{1/2}$ versus photon energy of TiO_2@AgCl samples: (a) TiAg-0, (b) TiAg-1, (c) TiAg-2, (d) TiAg-3, and (e) TiAg-4.
[Figura 5: $F(R(h\nu))^{1/2}$ versus energia do fóton de amostras de TiO_2@AgCl: (a) TiAg-0, (b) TiAg-1, (c) TiAg-2, (d) TiAg-3 e (e) TiAg-4.]

Emmett-Teller (BET) and the S_{BET} of TiO_2-anatase, TiO_2-rutile and prepared TiO_2 (TiAg-0) were found to be 52, 48 and 68 m^2/g, respectively (Table V).

Optical properties of TiO_2@AgCl: the variation of $F(R(h\nu))^{1/2}$ versus photon energy for the TiO_2@AgCl samples are shown in Fig. 5. The linear part of $F(R(h\nu))^{1/2}$ versus hν at higher photon energies indicates that the TiO_2@AgCl samples have indirect band transition. The linear portion of the curve, when extrapolated to zero, gives the optical bandgap value (Table VI). The measured optical bandgap values were in the range of 2.98 to 3.24 eV, which are very close to the bandgap of intrinsic TiO_2 powder and are in good agreement with the literature reports [37-39]. The presence of bandgap at 1.90, 1.94 and 2.26 eV in each sample of TiO_2@AgCl containing AgCl of 0.8, 2.6 and 4.4 wt%, respectively, whereas the presence of bandgaps at 1.98 and 1.88 eV in the sample of TiO_2@AgCl containing 9.4 wt% of AgCl were observed. These bandgap values were not related to the bandgaps from AgCl, because the bandgap values of AgCl are 3.25 eV for indirect bandgap and 5.60 for direct bandgap [40].

Table VI - Bandgap energy of TiO_2@AgCl samples.
[Tabela VI - Energias da banda proibida de amostras de TiO_2@AgCl.]

Sample code	Quantity of AgCl (wt%)	Bandgap (eV)		
		UV	Visible	
TiAg-0	0.0	3.14	-	-
TiAg-1	0.8	3.04	1.90	-
TiAg-2	2.6	3.24	1.94	-
TiAg-3	4.4	2.98	2.26	-
TiAg-4	9.4	3.02	1.98	1.88

CONCLUSIONS

The reflux technique under alkaline condition demonstrated the successful synthesis of AgCl-sensitized TiO_2 (TiO_2@AgCl). The TiO_2@AgCl was prepared from the precursor of TiO_2-rutile type which on its surface adsorb chloride anion (Cl^-) and various amounts of $AgNO_3$. The sample without the addition of $AgNO_3$ was analyzed by scanning electron microscope and surface area analyzer. The morphology of the sample without the addition of $AgNO_3$ showed a distribution of microspheres with approximately 0.5 to 1.0 μm and the specific surface area (S_{BET}) was 68 m^2/g. The crystal structure and optical properties of TiO_2@AgCl were investigated. The sample without the addition of $AgNO_3$ contained two types of TiO_2 phases, i.e. rutile

(major) and anatase (minor). The addition of $AgNO_3$ allowed the formation of AgCl phase and the reduction of rutile phase concentration. All treated samples indicated the same reflectance in the ultraviolet, while the samples with the addition of 0.8, 2.6, 4.4 and 9.4 wt% of AgCl indicated the same reflectance in the both the ultraviolet and visible spectrum. The bandgap energies of the samples were in the range of 2.97 to 3.24 eV, which are very close to the bandgap of intrinsic TiO_2 powder. The bandgaps at 1.90, 1.94 and 2.26 eV were observed in TiO_2@AgCl containing 0.8, 2.6 and 4.4 wt% of AgCl, respectively. Additionally, the bandgaps at 1.98 and 1.88 eV were verified for sample containing 9.4 wt% of AgCl.

ACKNOWLEDGEMENT

The authors are thankful to the Rector of Universitas Negeri Yogyakarta, Indonesia, for his support in the process of publication of this article.

REFERENCES

[1] C. Lu, H. Wu, R.B. Kale, J. Hazard Mater. **147** (2007) 213.
[2] Y. Chiba, A. Islam, Y. Watanabe, R. Komiya, N. Koide, L. Han, Jap. J. Appl. Phys. **45**, 25 (2006) L638.
[3] M. Farahmandjou, P. Khalili, Aust. J. Basic Appl. Sci. **7**, 6 (2013) 462.
[4] K. Gupta, R.P. Singh, A. Pandey, A. Pandey, Beilstein J. Nanotech. **4** (2013) 345.
[5] E.J. Wolfrum, J.M. Huang, D.M. Blake, P.C. Mannes, Z. Huang, J. Fiest, W.A. Jacoby, Environ. Sci. Technol. **36** (2002) 3142.
[6] T. Salthammer, F. Fuhrmann, Environ. Sci. Technol. **41** (2007) 6573.
[7] X.Z. Li, H. Liu, L.F. Cheng, H.J. Tong, Environ. Sci. Technol. **37**, 17 (2003) 3989.
[8] O. Carp, C.L. Huisman, A. Reller, Prog. Solid State Chem. **32** (2004) 33.
[9] J.F. Banfield, D.R. Veblen, Amer. Mineral. **77** (1992) 545.
[10] W.W. So, S.B. Park, K.J. Kim, C.H. Shin, S.J. Moon, J. Mater. Sci. **36** (2001) 4299.
[11] W. Wunderlich, T. Oekermann, L. Miao, N.T. Hue, S. Tanemura, M. Tanemura, J. Ceram. Process. Res. **4** (2004) 342.
[12] T. Gerfin, M. Gratzel, L. Walder, Prog. Inorg. Chem. **44** (1997) 345.
[13] C.G. Garcia, A.S. Polo, N.Y. Murakami Iha, Annals Brazilian Acad. Sci. **75**, 2 (2003) 163.
[14] J. Yu, M. Zhou, B. Cheng, H. Yu, X. Zhao, J. Mol. Catal. A: Chem. **227** (2004) 75.
[15] P. Wang, D. Wang, T. Xie, H. Li, M. Yang, X. Wei, Mater. Chem. Phys. **109** (2008) 181.
[16] J. Yu, L. Wu, J. Lin, P. Li, Q. Li, Chem. Commun. **13** (2003) 1552.
[17] H. Sutrisno, A. Ariswan, D. Purwaningsih. J. Math. Fund. Sci. **48**, 1 (2016) 82.
[18] J. Lynch, G. Giannini, J.K. Cooper, A. Loiudice, I.D. Sharp, R. Buosanti, J. Phys. Chem. C **119** (2015) 7443.
[19] S. Ramasamy, T. Ntho, M. Witcomb, M. Scurrell, Catal. Lett. **130** (2009) 341.
[20] H. Li, B. Zhu, Y. Feng, S. Wang, S. Zhang, W. Huang. J. Solid State Chem. **180**, 7 (2007) 2136.
[21] L. Yang, F. Wang, C. Shu, P. Liu, W. Zhang, S. Hu, Sci. Rep. **6** (2016) 21617.
[22] W. Sangchay, L. Sikong, K. Kooptamond, Proc. Eng. **32** (2012) 590.
[23] M. Evain, U-Fit v1.3, Inst. Mater. Nantes, Nantes, France (1995).
[24] S. Brunauer, P.H. Emmett, E. Teller, J. Amer. Chem. Soc. **60**, 2 (1938) 309.
[25] H.P. Klug, L.E. Alexander, *X-ray diffraction procedures for polycrystalline and amorphous materials*, John Wiley & Sons, New York (1954).
[26] C.R. Hubbard, R.L. Snyder, Powder Diffr. **3**, 2 (1988) 74.
[27] P. Kubelka, J. Optic. Soc. Amer. **38**, 5 (1948) 448.
[28] P. Kubelka, F. Munk, Z. Tech. Phys. (Leipzig) **12** (1931) 593.
[29] S. Tandon, J. Gupta, Phys. Status Solidi **38** (1970) 363.
[30] K. Sreen, C. Poulose, B. Unni, Solar Energy Mater. Solar Cells **92** (2008) 1462.
[31] A.E. Morales, M.E. Sanchez, U. Pal, Rev. Mex. Fis. **53**, 5 (2007) 18.
[32] C. Ting, S. Chen, J. Appl. Phys. **88** (2000) 4628.
[33] K. Sugiyama, Y. Takeuchi, Kristallographie **194** (1991) 305.
[34] L.I. Bekkerman, I.P Dobrovol'skii, A.A. Ivakin, Russ. J. Inorg. Chem. **21** (1976) 223.
[35] K.I. Khitrova, M.F. Bundule, Z.G. Pinsker, Kristallografiya **22** (1977) 253.
[36] H.E. Swanson, R.K. Fuyat, G.M. Ugrinic, Natl. Bur. Stand. Circ. **4** (1955) 539.
[37] R. Nainani, P. Thakur, M. Chaskar, J. Mater. Sci. Eng. B **2**, 1 (2012) 52.
[38] D.O. Scanlon, C.W. Dunnill, J. Buckeridge, S.A. Shevlin, A.J. Logsdail, S.M. Woodley, C.R.A. Catlow, M.J. Powell, R.G. Palgrave, I.P. Parkin, G.W. Watson, T.W. Keal, P. Sherwood, A. Walsh, A.A. Sokol, Nat. Mater. **12** (2013) 798.
[39] V. Pfeifer, P. Erhart, S. Li, K. Rachut, J. Morasch, J. Brötz, P. Reckers, T. Mayer, S. Rühle, A. Zaban, I.M. Seró, J. Bisquert, W. Jaegermann, A. Klein, J. Phys. Chem. Lett. **4** (2013) 4182.
[40] J. Tejeda, N.J. Shevchik, W. Braun, A. Goldmann, M. Cardona, Phys. Rev. B **12** (1975) 1557.
(Rec. 31/05/2017, Rev. 21/07/2017, 23/08/2017, Ac. 04/09/2017)